ACS APPLIED MATERIALS & INTERFACES

Research Article

www.acsami.org

Structural Evolution during Mechanical Deformation in High-Barrier PVDF-TFE/PET Multilayer Films Using in Situ X-ray Techniques

Alex M. Jordan,[†] William R. Lenart,[†] Joel M. Carr,[†] Eric Baer,[†] and LaShanda T. J. Korley*[,†]

[†]Center for Layered Polymeric Systems, Department of Macromolecular Science and Engineering, Case Western Reserve University, Cleveland, Ohio 44106-7202, United States

Supporting Information

ABSTRACT: Poly(vinylidene fluoride-*co*-tetrafluoroethylene) (PVDF-TFE) is confined between alternating layers of poly(ethylene terephthalate) (PET) utilizing a unique multilayer processing technology, in which PVDF-TFE and PET are melt-processed in a continuous fashion. Postprocessing techniques including biaxial orientation and melt recrystallization were used to tune the crystal orientation of the PVDF-TFE layers, as well as achieve crystallinity in the PET layers through strain-induced crystallization and thermal annealing during the melt recrystallization step. A volume additive model was used to extract the effect of crystal orientation within the PVDF-TFE layers and revealed a significant enhancement in the modulus from 730 MPa in the as-extruded state (isotropic) to 840 MPa in the biaxially oriented state (on-edge) to 2230 MPa in the melt-recrystallized state (in-plane). Subsequently, in situ wide-angle X-ray scattering was used to observe the crystal structure evolution during uniaxial deformation in both the as-extruded and melt-recrystallized states. It is observed that the low-temperature ferroelectric PVDF-TFE crystal phase in the as-extruded state exhibits equatorial sharpening of the 110 and 200 crystal peaks during deformation, quantified using the Hermans orientation function, while in the melt-recrystallized state, an overall increase in the crystallinity occurs during deformation. Thus, we correlated the mechanical response (strain hardening) of the films to these respective evolved crystal structures and highlighted the ability to tailor mechanical response. With a better understanding of the structural evolution during deformation, it is possible to more fully characterize the structural response to handling during use of the high-barrier PVDF-TFE/PET multilayer films as commercial dielectrics and packaging materials.

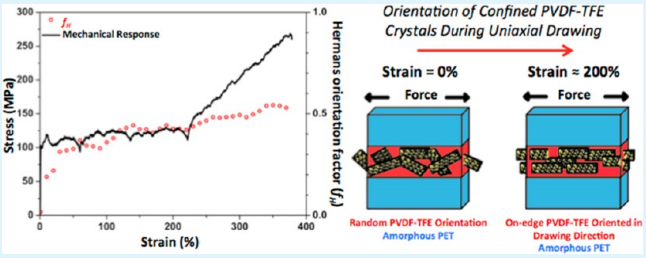

KEYWORDS: *in situ deformation, thin films, mechanical properties, multilayer coextrusion, confined crystallization, biaxial orientation, isothermal recrystallization*

INTRODUCTION

Confinement of semicrystalline polymers has been widely investigated with respect to the induced morphological changes, which significantly affect their mechanical,[1−6] electrical,[7−9] and gas-barrier properties.[10−12] Traditional confinement methods include spin coating,[2,3] template wetting,[13,14] electrospinning,[15,16] and block copolymer synthesis.[17] Spin coating, template wetting, and electrospinning all require the use of solvents, which limits the application of these techniques.[2,3] Block copolymers containing at least one semicrystalline segment have also been utilized to produce confined systems; however, synthetic complexity and compatibility limit the possible combinations of polymers.[11] One of the most successful and promising methods for producing confined systems is forced-assembly, multilayer coextrusion. This process uses layer-multiplying dies that consecutively split, spread, and then stack immiscible polymer layers in an ABABAB configuration for a two-component system. It is also possible to introduce an additional polymer layer to produce a three-component system in an ABCABC configuration or use it as a tie layer in an ATBTA configuration. This process is capable of producing layered films containing from 2 to 4096 layers, and eliminates exposed (free) surfaces in the confined polymer with specific control of the confined layer thickness.[18,19] Therefore, multilayer coextrusion provides an opportunity for one-dimensional (1D) semicrystalline polymer confinement that controls surface energetics, eliminates solvents, and is easily scaled to industrial levels.

Because of its resolution scale and fast scan times, synchrotron radiation has proven to be an invaluable tool for studying in situ polymeric structures.[20] For instance, near the glass transition temperature (T_g) of poly(ethylene terephthalate) (PET), this method has been utilized to probe its crystal structure development because of its fast exposure times and detailed resolution.[21−23] Confinement-induced crystallization of poly(vinylidene fluoride) (PVDF) has also been studied using this technique, which allowed researchers to observe nanoscale PVDF structures.[24] Previously, we reported coextrusion processing of PET and poly(vinylidene fluoride-*co*-tetrafluoroethylene) PVDF-TFE, a copolymer similar to PVDF, and its

Received: November 26, 2013
Accepted: February 18, 2014
Published: March 4, 2014

   dx.doi.org/10.1021/am4053893 | *ACS Appl. Mater. Interfaces* 2014, 6, 3987−3994

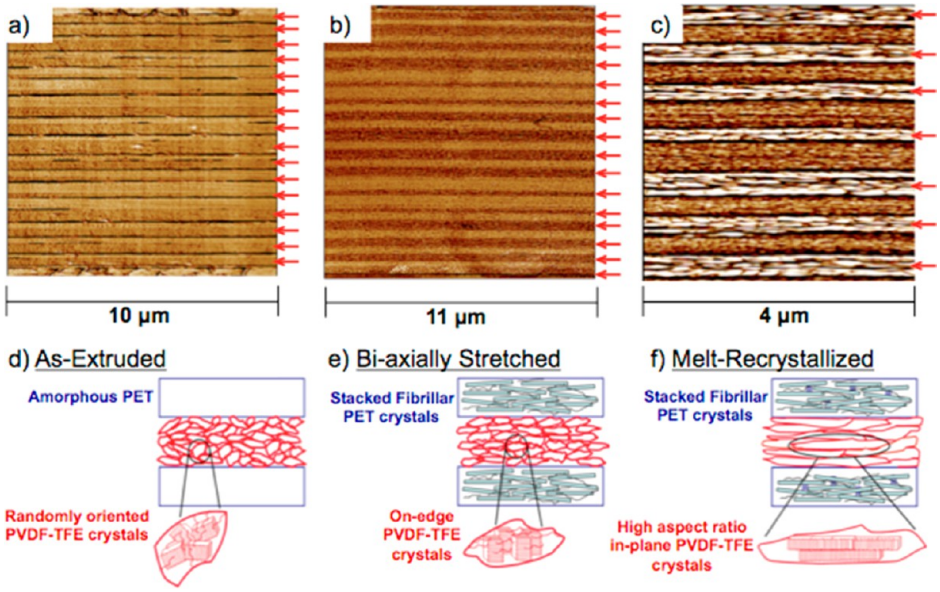

Figure 1. Atomic force microscope images of (a) as-extruded, (b) biaxially stretched, and (c) melt-recrystallized 50:50 PET/PVDF-TFE 32-layer composites, with red arrows indicating PVDF-TFE layers. Schematic representations of the crystal structures formed in (d) as-extruded, (e) biaxially stretched, and (f) melt-recrystallized systems. Reprinted with permission from ref 26. Copyright Elsevier 2013.

subsequent biaxial orientation and melt recrystallization in multilayer films. In the as-extruded state, PVDF-TFE layers showed a random crystal orientation, and the PET layers formed an amorphous phase. In the biaxially stretched state, the PVDF-TFE layers exhibited an on-edge crystal orientation, while PET layers underwent strain-induced crystallization, exhibiting a stacked-oriented fibrillar structure. Following melt recrystallization, the PVDF-TFE layers exhibited an in-plane crystal orientation, while the PET layers were further crystallized.[25,26]

The shift in crystal orientation is analogous to the shift observed by Wang et al. in multilayer films of poly(ethylene oxide) (PEO) and poly(ethylene-*co*-acrylic acid) (EAA) strictly through confinement. In thick layers, PEO formed randomly oriented crystals, similar to the as-extruded PVDF-TFE; as the layer thickness decreased, the PEO crystal orientation shifted to a single-crystal-like, in-plane structure, similar to the melt-recrystallized PVDF-TFE.[27] As a result of this similarity, we will draw a number of comparisons between our PET/PVDF-TFE composite and this examination of the same EAA/PEO composite films to elucidate the effect of postprocessing techniques on the observed mechanical response of the PET/PVDF-TFE composite system.[10,27]

The controlled morphology of the PVDF-TFE layers confined between PET in multilayer systems was found to dramatically impact both oxygen and water permeability properties in addition to energy storage and dielectic properties.[28] By utilizing the PET/PVDF-TFE system with these postprocessing techniques, we have distinct control over the morphology of the system compared to the reported examination of the EAA/PEO system, where single-crystal-like morphology was achieved strictly through confinement. Lai et al. demonstrated that, as thick PEO crystals deformed, on-edge 120 crystals were formed and the thin PEO in-plane single crystals underwent recrystallization during deformation.[10] An understanding of the effect of postprocessing techniques on the mechanical properties of these complex systems is crucial to optimization of the biaxial orientation and melt recrystallization to tune the mechanical properties of confined crystallization systems; the mechanical response of these films will directly impact their use (e.g., permeability, breakdown) as dielectric materials. Using wide-angle X-ray scattering (WAXS) powered by synchrotron radiation, this study further probes these PET/PVDF-TFE multilayer films by examining their mechanical properties and the unique confined crystal structure of PVDF-TFE during deformation to provide insight into the observed mechanics.

EXPERIMENTAL SECTION

Materials. PET, commercially known as Polyclear 1101q (inherent viscosity = 0.83), was obtained from Invista Polymers and Resins and dried at 80 °C for 24 h before melt processing. PVDF-TFE, known as Neoflon VP-50, was obtained from Daikin Industries, Ltd., and contains 20 mol % TFE. Multilayer films were produced at an extrusion temperature of 260 °C with a cooled steel chill roll temperature of 70 °C using previously reported techniques.[29] A skin layer of polyethylene (PE; Dow Chemical, DOW LDPE 5005) was laminated on either side of the PET/PVDF-TFE multilayer films to protect against damage and was subsequently delaminated before testing and postprocessing.[26]

Postprocessing Techniques. The films in the as-extruded state remained unmodified after the multilayer coextrusion process. Films in the biaxially stretched state were stretched to a 4.5 × 4.5 ratio at a rate of 100% s^{-1} at a temperature of 105 °C on a Brückner (Greenville, SC, and Siegsdorf, Germany) Karo IV laboratory-scale stretcher to produce on-edge PVDF-TFE crystals, with the same layer and overall film thickness as those of the as-extruded films.[26] This temperature was chosen because it is above the T_g value of PET at 75 °C but below the melting temperature (T_m) of PVDF-TFE. In order to produce the melt-recrystallized system, the biaxially stretched films were heated to 140 °C (between the T_m values of PVDF-TFE and PET) in a mineral oil bath for 20 min, then cooled to 120 °C, and held isothermally for 3 h to produce in-plane PVDF-TFE crystals. During the melt recrystallization procedure, the multilayer films were placed in an open fixture and held under tension.

Uniaxial Mechanical Analysis. Uniaxial tensile deformation was performed on a Zwick/Roell mechanical testing instrument with a 500 N load cell at room temperature and a constant strain rate of 10% min^{-1}. Samples were cut from 8 μm-thick films using a dog-bone (16

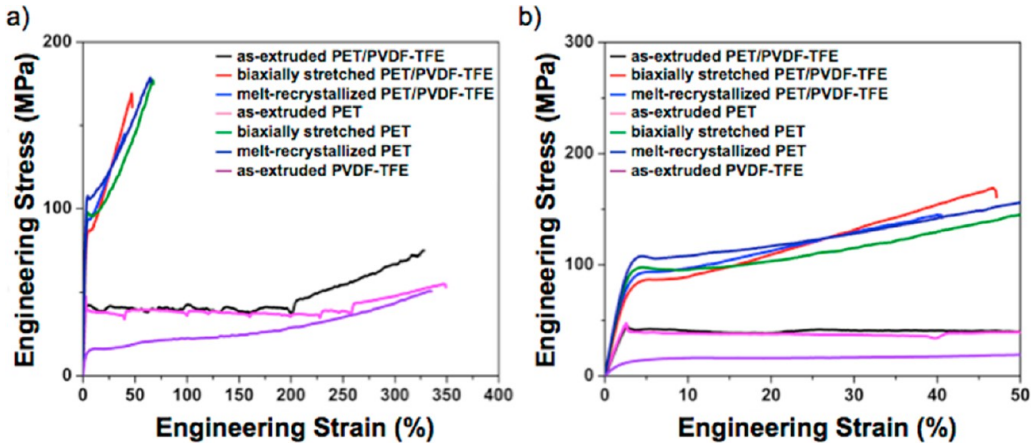

Figure 2. Representative stress–strain curves for the 256-layer, 70:30 volume composition PET/PVDF-TFE multilayer films and controls for the as-extruded, biaxially stretched, and melt-recrystallized systems: (a) entire stress–strain response; (b) low-strain response (<50%) shown for clarity in the postprocessed systems.

mm × 2.08 mm) steel die according to ASTM D638 with a minimum of five samples per layer thickness and volume composition.[30] The samples were placed between Mylar sheets during cutting to relieve stress concentration at the edges of the die and then smoothed with a polishing cloth to remove defects.

In Situ Deformation Analysis. Synchrotron measurements were carried out at Brookhaven National Laboratory (BNL) National Synchrotron Light Source (NSLS) at the X27C beamline. The two-dimensional (2D) WAXS patterns were recorded on a Bruker Smart 1500 X-ray CCD detector (resolution 1024 × 1024 pixels) at a wavelength of 0.1371 nm. The sample-to-collector distance was calibrated using an Al_2O_3 standard with an *012* reflection at 2θ = 22.70° and a *104* reflection at 2θ = 31.14° to yield a final sample-to-collector distance of 126.2 mm. In situ deformation studies were also conducted at a strain rate of 10% min^{-1} on a tensile stage. Images were collected every 1 min to allow for adequate exposure time while minimizing stress relaxation effects, with the beam striking perpendicular to the layers (normal direction). All X-ray images were processed using "POLAR" software (Stonybrook Technology and Applied Research, Inc.).

RESULTS AND DISCUSSION

The layer integrity and structure within the as-extruded, biaxially stretched, and melt-recrystallized PET/PVDF-TFE films have been previously examined[26] and are reviewed in Figure 1. The layer integrity is maintained during the postprocessing biaxial stretching, as well as in subsequent melt recrystallization (Figure 1a–c). It should also be noted that it is possible to observe high-aspect-ratio in-plane single-crystal-like structures in the PVDF-TFE layers in the melt-recrystallized system (Figure 1c). The schematics in Figure 1d–f represent the crystal structures formed at each stage of processing. The randomly oriented PVDF-TFE crystal structure is depicted in Figure 1d, and Figure 1e represents the on-edge crystal structure in the PVDF-TFE layers and the development of a stacked fibrillar crystal structure in the PET layers. Figure 1f shows the formation of high-aspect-ratio, in-plane crystals developed in the melt-recrystallized system.

Mechanical testing was performed on as-extruded, biaxially stretched, and melt-recrystallized PET/PVDF-TFE multilayer films at 50:50 and 70:30 volume compositions with 32 and 256 layers, respectively, to correlate the mechanical response of the films to the confined crystal structure developed in the PVDF-TFE layers. There was no significant shift in the mechanical properties as the layer thickness and the number of layers were changed; this comprehensive mechanical investigation is tabulated in Tables S1–S3 in the Supporting Information (SI) and shown in Figures S1–S3 in the SI. Because the PVDF-TFE crystal structure did not change with the layer thickness in the as-extruded state, as evidenced by our previous permeability study, this result is to be expected.[26] As a result, we chose to focus on the mechanical response of the 256-layer, 70:30 system (Figure 2 and Table 1).

Table 1. Tabulated Mechanical Properties of the Selected 256-Layer, 70:30 Volume Composition Multilayer Films and Controls in the As-Extruded, Biaxially Stretched, and Melt-Recrystallized Systems

sample	E_T (MPa)	UTS (MPa)	ε_b (%)
as-extruded PVDF-TFE	730 ± 40	48.8 ± 2.3	330 ± 10
as-extruded PET	1860 ± 130	57.7 ± 6.4	340 ± 30
biaxially stretched PET	3440 ± 210	190 ± 16	67.4 ± 2.1
melt-recrystallized PET	4160 ± 320	170 ± 14	53 ± 13
as-extruded PET/PVDF-TFE	1800 ± 120	75.2 ± 1.2	340 ± 20
biaxially stretched PET/PVDF-TFE	2660 ± 110	168 ± 15	46.1 ± 5.9
melt-recrystallized PET/PVDF-TFE	3580 ± 290	147 ± 3	33.7 ± 5.2

Figure 2a details the entire stress–strain tensile response of the 256-layer, 70:30 composition system, while Figure 2b highlights the same curves in the region of strains less than 50% for clarity in the biaxially stretched and melt-recrystallized states. Because both the biaxially stretched and melt-recrystallized systems have been drawn to a 4.5 × 4.5 ratio (well past the linear elastic region) as a result of postprocessing, they do not achieve a strain-at-break (ε_b) as high as the as-extruded state (340 ± 20%), only stretching to 46.1 ± 5.9% and 53 ± 15%, respectively. In the linear elastic region, it is possible to directly observe the enhancement in rigidity that accompanies the morphological shift from randomly oriented crystals to on-edge crystals to in-plane, pseudo-single-crystal structures in the PVDF-TFE layers as well as the oriented fibrillar structure in the PET layers developed during postprocessing. The elastic modulus (E_T) of the composite multilayer film increases from 1800 ± 120 MPa in the as-extruded state (randomly oriented PVDF-TFE crystals/amorphous PET) to 2660 ± 110 MPa in the biaxially stretched (on-edge PVDF-TFE crystals/oriented

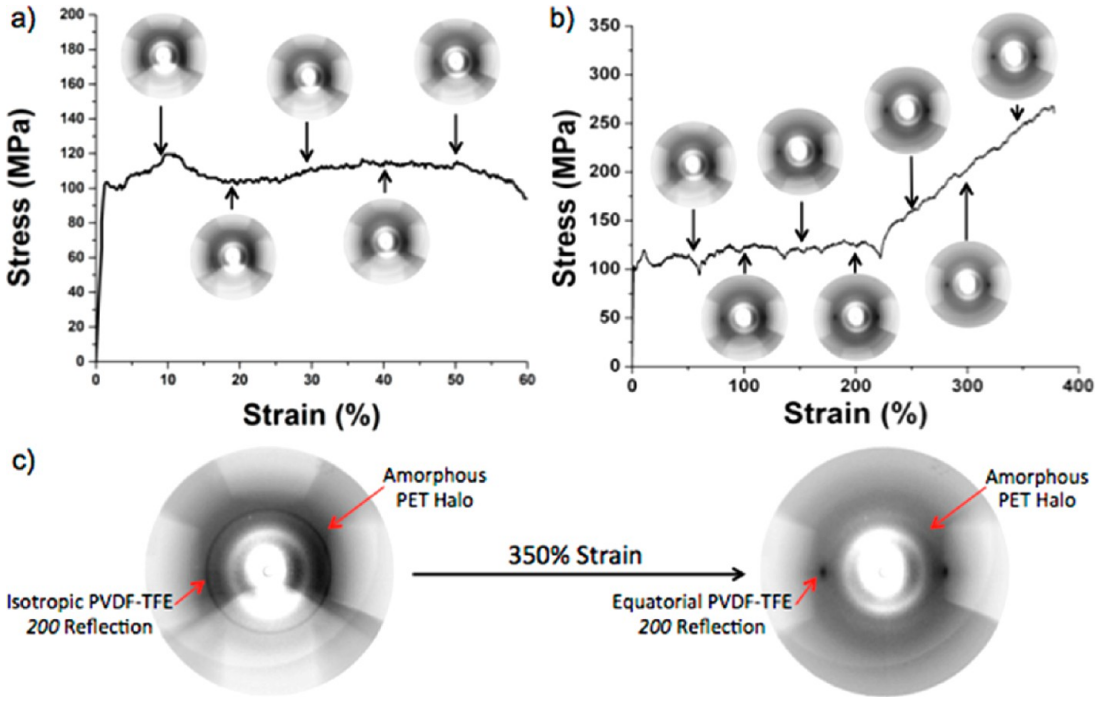

Figure 3. (a) Low-strain (less than 60%) stress–strain curve with corresponding WAXS patterns every 10%. (b) Entire stress–strain curve with WAXS patterns every 50%. (c) Initial and final collected at 0% and 380% elongation.

PET fibrils) state and increases even further to 3580 ± 290 MPa in the melt-recrystallized (in-plane, single-crystal PVDF-TFE layers/stacked-oriented PET fibril crystals) state. Post-processing effects the morphologies of both the PET and PVDF-TFE layers, which causes this dramatic shift in the mechanical properties; the effect of postprocessing on the modulus of the PVDF-TFE layers will be isolated and discussed in detail later. However, both the biaxially stretched and melt-recrystallized films achieve an ultimate tensile strength (UTS) approximately twice as high as that of the as-extruded films because of postprocessing-induced on-edge and in-plane morphologies, respectively. It should be noted that after deviating from linear elastic deformation, the force (stress) required to continually deform the melt-recrystallized, single-crystal-like system is higher than that of the biaxially stretched on-edge crystal system. Thus, the similarity in the UTS arises from the difference in ε_b between the biaxially stretched and melt-recrystallized systems. It is also noted that all of the PET/PVDF-TFE multilayer systems exhibit characteristic strain-induced hardening phenomena. In the as-extruded composite, there is a distinct cold-drawing region where the sample begins to neck before the observed strain-hardening region, which has an onset of around 200% strain, while the biaxially stretched and melt-recrystallized composites begin strain hardening immediately after yielding. These phenomena will be discussed with more detail in a later section.

$$E_{\text{PVDF-TFE}} = \frac{E_{\text{composite}} - \varphi_{\text{PET}} E_{\text{PET}}}{\varphi_{\text{PVDF-TFE}}} \quad (1)$$

Because it was possible to obtain biaxially stretched and melt-recrystallized PET controls, an additive model (eq 1) was used to isolate and determine the modulus of the PVDF-TFE layers and to investigate the effect of the PVDF-TFE crystal orientation in accordance with the work of Lai et al.[11] To determine whether this model properly fits the system, as-extruded controls of both PET and PVDF-TFE were used to calculate a theoretical E_T of approximately 1520 MPa, which was then compared to the experimentally obtained modulus of 1800 ± 120 MPa. When the error in the control measurements is considered, these values are within reasonable agreement, allowing this additive model to be extended to the biaxially stretched and melt-recrystallized films, using the respective biaxially stretched PET (E_{PET} = 3440 ± 210 MPa) and melt-recrystallized PET (E_{PET} = 4160 ± 320 MPa) controls. As such, the influence of the PET layers, and their corresponding morphologies, on the modulus can be extracted, which allows evaluation of only the relationship between the crystal orientations within the PVDF-TFE layer and observed modulus. This volume additive model approach has also been used with success in determining the permeability of the individual PVDF-TFE layers in our previous work.[26]

Further evaluation of the multilayer PET/PVDF-TFE films via the additive model revealed significant modulus changes with PVDF-TFE crystal orientation. Compared to the randomly oriented, as-extruded multilayered systems, the biaxially stretched films with on-edge orientation exhibited an incremental enhancement (15%) in the PVDF-TFE layer modulus, increasing from 730 MPa in the as-extruded films to 840 MPa for the biaxially stretched film in the 70:30 composition, 256-layer system. A much more dramatic modulus increase was observed for the melt-recrystallized PVDF-TFE films, which exhibited in-plane, high-aspect-ratio crystals. This highly oriented PVDF-TFE crystal structure resulted in an effective PVDF-TFE layer modulus of 2230 MPa, which is an increase of approximately 205% compared to the random orientation exhibited in the as-extruded system. We propose that this remarkable enhancement of the PVDF-TFE layer modulus can be attributed to the increased interchain interactions and pseudo-single-crystal orientation of the PVDF-TFE crystal structure. This result is in agreement with that previously observed in confined PEO, the modulus of the PEO

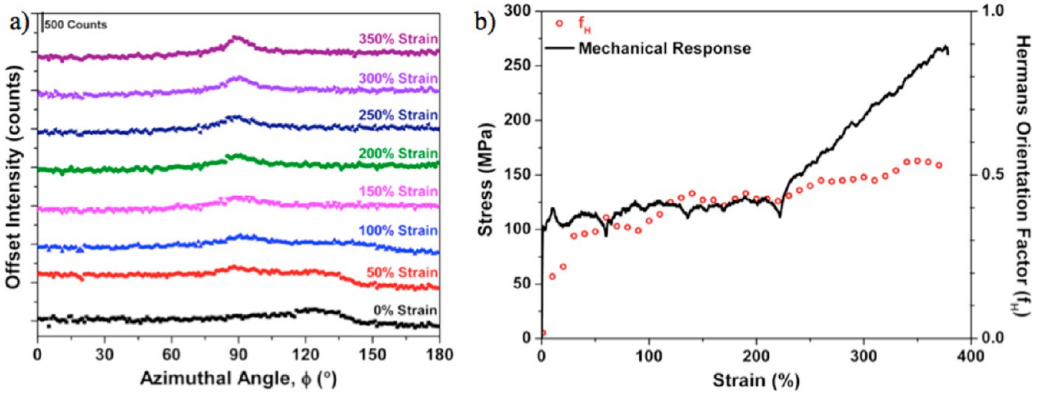

Figure 4. (a) Azimuthal intensity scans of the PVDF-TFE crystal peak. (b) Breadth taken from the full width at half-maximum of the azimuthal scan. (c) Height of the azimuthal peak.

layers significantly increased as the crystal orientation in the PEO layers shifted from a random isotropic orientation to in-plane crystals. In the bulk with randomly oriented PEO crystal layers, the PEO modulus was 428 ± 38 MPa. By forming single-crystal-like, oriented PEO crystals, the PEO layer modulus increased to 1450 ± 99 MPa, an increase of approximately 240%.[10]

To examine the role of the crystal structure and molecular arrangement on the mechanical properties of the PET/PVDF-TFE films, in situ X-ray studies were performed during the deformation process. While both PVDF-TFE and PET are capable of crystallizing during drawing, it is widely known that PET crystallizes following drawing at elevated temperatures above its T_g, while stretching below the T_g value of PET forms an amorphous glass phase.[31] Our studies were conducted at ambient conditions, which did not allow PET to alter its crystal structure during deformation. This approach allowed us to examine the evolution of unique confined crystal structures in the PVDF-TFE layers during in situ deformation studies, while the PET layers remained amorphous in the as-extruded study and were held in an oriented fibril crystal structure in the melt-recrystallized study similar to observations in bulk PET (both as-extruded and melt-recrystallized states). For the purpose of this study, the as-extruded and melt-recrystallized samples were examined using in situ WAXS to allow examination of the extremes of the postprocessing conditions on the crystal structure of the PVDF-TFE and PET layers.

In the as-extruded state, we observed an isotropic scattering pattern (Figure 3), consistent with results obtained in our previous work focused on the barrier properties, and confirming that the sample being studied had the same random crystal orientation in the PVDF-TFE layers, with a significant amorphous halo attributed to the PET layers.[26] The isotropic pattern appears at $2\theta = 17.7°$ and represents the *200* and *110* crystal reflections for PVDF-TFE. Consequently, we are able to isolate this reflection to probe the crystal structure evolution of only the PVDF-TFE layers.

The PET/PVDF-TFE multilayer films achieved an elongation-at-break of 383% during the deformation study and exhibited the same characteristic stress–strain response as those tested during the mechanics study, allowing a direct correlation of the results. Figure 3a shows the low-strain region (less than 60%) of the as-extruded film along with the WAXS pattern obtained at these low strains. It can be seen that the scattering pattern remains isotropic, but following the first stress relaxation event at approximately 60% strain, the isotropic peak begins to shift to a well-defined equatorial reflection, shown in Figure 3b and in greater detail in Figure 3c, where the reflection is clearly seen within the PET amorphous halo. This observed sharpening of the PVDF-TFE crystal reflection is indicative of a higher ordering of the PVDF-TFE crystals into an on-edge structure oriented in the stretching plane, quantifiable using the Hermans orientation function, f_H (eq 2). In understanding f_H, values range from −0.5 for crystals oriented perpendicular to the *c* axis (extrusion direction) to unity for crystals oriented parallel to the extrusion direction.[32]

$$f_H = \frac{3\langle \cos^2 \phi \rangle_c - 1}{2} \tag{2}$$

The azimuthal angle, ϕ, is defined with respect to the meridian of the WAXS pattern. In order to utilize the major *110* and *200* reflections, $\langle \cos^2 \phi \rangle_c$ is calculated using eq 3, where perpendicular reflections along the *hk0* axis are used.[33]

$$\langle \cos^2 \phi \rangle_c = 1 - 2\langle \cos^2 \phi \rangle_{hk0} \tag{3}$$

To determine this *hk0* cosine value, eq 4 is used, where $I(\phi)_{hk0}$ is the intensity of the *hk*0 reflections at each azimuthal angle, ϕ.[32,33]

$$\langle \cos^2 \phi \rangle_{hk0} = \frac{\int_0^{\pi/2} I(\phi)_{hk0} \sin \phi \cos^2 \phi \, d\phi}{\int_0^{\pi/2} I(\phi)_{hk0} \sin \phi \, d\phi} \tag{4}$$

Shown in Figure 4a are select offset azimuthal scans from 0° < ϕ < 180°. It can be seen that the intensity along the equator for the *110* and *200* reflections sharpens at strains of approximately 200%. The mechanical response of the as-extruded multilayer film obtained during the in situ deformation study is then overlaid with the calculated f_H values from the WAXS profiles obtained during the experiment in Figure 4b. The increasing orientation along the extrusion/stretching direction is clearly visible, as the values for f_H begin at 0.02, corresponding to an isotropic reflection pattern (Figure 3c, left) and slowly increase to a final value of approximately 0.56 at a strain of 370% prior to sample failure. This observation indicates that, during the uniaxial deformation process, PVDF-TFE crystals are oriented along the drawing (extrusion) direction.[32] Although both the PVDF-TFE and PET as-extruded controls exhibit a strain-hardening phenomena, the magnitude of strain hardening in the multilayer film is much more pronounced than either control, as shown in Figure 2a. As a result of this study, we attribute the enhanced strain-hardening behavior of the PET/

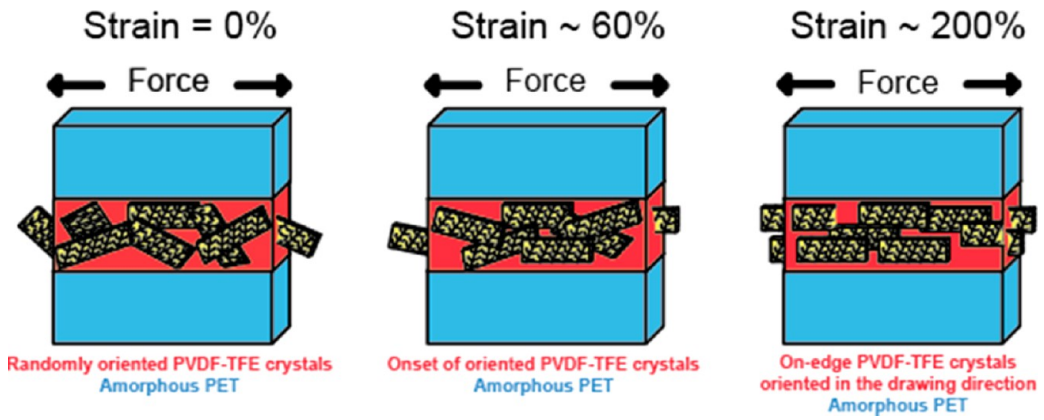

Figure 5. Schematic representation of the progression from randomly oriented PVDF-TFE crystals confined by amorphous PET layers in the as-extruded state to on-edge PVDF-TFE crystals oriented in the drawing direction (applied force).

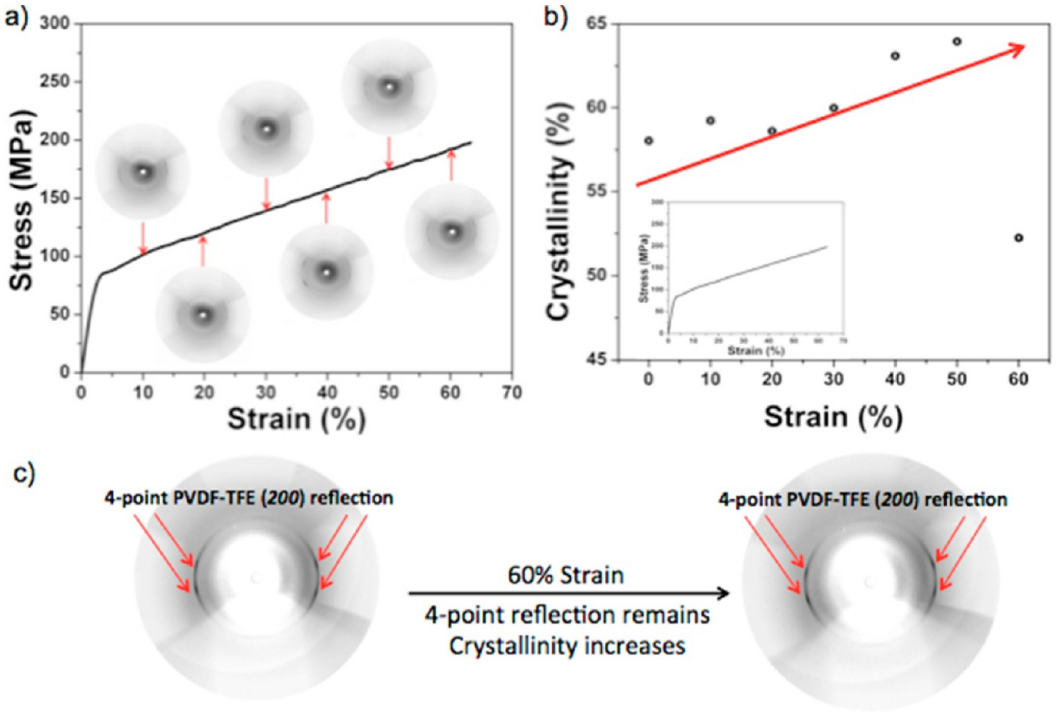

Figure 6. (a) Stress–strain curve of the melt-recrystallized PET/PVDF-TFE multilayer film with the obtained WAXS pattern every 10% strain. (b) Calculated percent crystallinity plotted against strain. (c) Initial and final WAXS pattern collected with clearly visible four-point 200 PVDF-TFE reflections present.

PVDF-TFE multilayer films to the increased chain alignment along the extrusion direction because the PET layers remained amorphous during deformation with a structure similar to that of bulk PET.

This result is in agreement with the prior art using PEO/EAA multilayer films. In films with thick layers (>510 nm), PEO formed random spherulites, analogous to the randomly oriented PVDF-TFE crystals in the as-extruded state. Upon uniaxial deformation, a progression was observed from isotropic PEO crystal to oriented crystals along the drawing axis, as evidenced by a sharpening of the *120* PEO crystal reflections.[10] A graphical representation of the progression from randomly oriented *110* and *200* PVDF-TFE crystals in the undrawn as-extruded state to on-edge crystals oriented in the drawing direction is shown in Figure 5.

The melt-recrystallized PET/PVDF-TFE multilayer films, which contain in-plane-oriented PVDF-TFE crystals and oriented PET fibril crystals, were then evaluated as an extreme comparison to the as-extruded PET/PVDF-TFE films. As the melt-recrystallized sample is deformed, strain hardening occurs (Figures 2 and 6a) immediately after plastic deformation begins, compared to the as-extruded state where strain hardening does not occur until almost 250% strain. During tensile deformation, real-time crystallographic information on the PVDF-TFE and PET crystals (Figure 6a) was obtained. Peak deconvolutions were performed using a Gaussian fit with nonlinear least-squares regression (Figure S4 in the SI).

While both PVDF-TFE and PET crystals are present, the PVDF-TFE *200* and *110* reflections are clearly distinguishable in the 2D WAXS pattern. Thus, we are again able to isolate and examine the effect of deformation on the PVDF-TFE crystal structure of the melt-recrystallized multilayer films. The melt-recrystallized multilayer film examined in this study exhibited equatorial reflections for the *110* and *200* reflections in a four-

point pattern at all strains during deformation up to an ε_b of 64% (Figure 6a,c), implying that the crystals maintained a single-crystal-like, in-plane morphology during deformation. This is in contrast to the equatorial reflections observed during deformation of the as-extruded films, which transformed from an isotropic ring (in the unstretched state) to a distinct, sharp equatorial reflection upon deformation. This would imply that, unlike the as-extruded multilayer film where the PVDF-TFE crystals shifted from a random orientation to align as on-edge crystals in the stretching direction during deformation, the orientation of the PVDF-TFE crystals in the melt-recrystallized state is static during deformation. The calculated crystallinity (Figure 6b) decrease at 60% strain is most likely due to incomplete collection of the sample scan, resulting from data collection parameters.

$$\%\ \text{crystallinity} = \frac{A_c}{A_a + A_c} \times 100\% \quad (5)$$

It is possible to integrate the deconvoluted peaks from the 1D WAXS pattern to obtain the contribution to the total scattering from both the crystal (A_c) and amorphous (A_a) regions, which can be utilized to determine the relative percent crystallinity according to eq 5. The crystallinity of the film increases upon deformation from 56% in the initial state, up to 64% on the same sample before failure (Figure 6b). Because the crystal structure did not change during deformation, we propose that an overall increase in the crystallinity is responsible for the observed strain-hardening behavior, as shown in Figure 7. It is

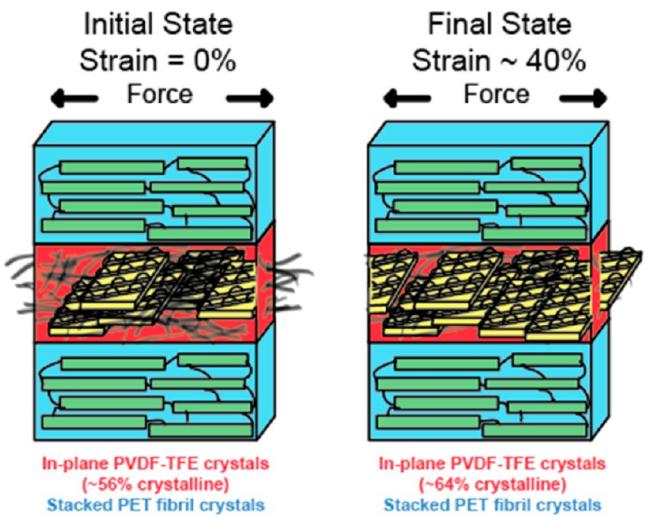

Figure 7. Schematic representation of the evolution of the in-plane crystal structure of PVDF-TFE crystals confined between crystallized PET fibrils.

widely known that as the crystallinity of a material increases, so does the force required to deform the sample, correlating to a strain hardening phenomena.[34,35] Thus, we attribute the strain hardening phenomena observed to this increase in crystallinity in the melt-recrystallized system.

Again, we find that our results agree with the previous study of PEO/EAA multilayer films with thin (<125 nm) layers, where the PEO layers formed single-crystal-like in-plane morphologies. A strain-induced recrystallization phenomenon was observed with the PEO single-crystal system, while retaining a high proportion of in-plane crystal orientation during deformation.[10] With individual PVDF-TFE layer thicknesses of approximately 20 nm, we also attribute the fact that the crystals remain in-plane to spatial restriction and mechanical reinforcement from the crystals during deformation.

CONCLUSION

Through confinement of PVDF-TFE between alternating layers of PET and utilization of biaxial orientation and melt recrystallization, the modulus of confined PVDF-TFE increases 15% and 200%, respectively. Using PET as a confining layer allows for visualization of the crystal structure of PVDF-TFE via real-time in situ deformation in the as-extruded as well as melt-recrystallized state, and it is shown that a sharpening of the PVDF-TFE crystal peak correlates to the strain-hardening behavior of the multilayer films in the as-extruded state. Subsequently, it is shown that an overall increase in strain-induced PVDF-TFE crystallization is responsible for the strain-hardening phenomenon in the melt-recrystallized films. Postprocessing techniques have proven valuable for tuning the mechanical response of multilayer films, and in situ WAXS analysis has allowed us to probe structural development during deformation of confined semicrystalline polymers to explore these structure−property relationships.

ASSOCIATED CONTENT

Supporting Information

Detailed mechanical analysis of the effect of the number of layers and layer thickness on the as-extruded, biaxially stretched, and melt-recrystallized PET/PVDF-TFE multilayer films, which are shown to be negligible, and details of the peak deconvolution performed on the melt-recrystallized in situ WAXS tensile data utilizing *Origin* software can be found in the SI. This material is available free of charge via the Internet at http://pubs.acs.org.

AUTHOR INFORMATION

Corresponding Author

*Phone: (216) 368-1421. E-mail: lashanda.korley@case.edu.

Notes

The authors declare no competing financial interest.

ACKNOWLEDGMENTS

The authors thank Jesse Gadley for his assistance in data collection and Dr. Chuan-Yar Lai for her helpful discussions on the deformation mechanics in multilayer films. The authors acknowledge support from the National Science Foundation Science and Technology Center for Layered Polymeric Systems (Grant DMR-0423914) and use of beamline X27C at BNL NSLS through the U.S. Department of Energy under Contract DE-AC02-98CH10886. We also acknowledge funding from the Defense University Research Instrumentation Program (Grant W911NF1110343) and the Office of Naval Research (Grant N00014-10-1-0349).

REFERENCES

(1) Jeon, K.; Krishnamoorti, R. Morphological Behavior of Thin Linear Low-Density Polyethylene Films. *Macromolecules* **2008**, *41* (19), 7131−7140.

(2) Wang, Y.; Chan, C. M.; Ng, K. M.; Li, L. What Controls the Lamellar Orientation at the Surface of Polymer Films during Crystallization? *Macromolecules* **2008**, *41* (7), 2548−2553.

(3) Hu, Z.; Baralia, G.; Bayot, V.; Gohy, J. F.; Jonas, A. M. Nanoscale Control of Polymer Crystallization by Nanoimprint Lithography. *Nano Lett.* **2008**, *5* (9), 1738−1743.

(4) Burt, T. M.; Keum, J.; Hiltner, A.; Baer, E.; Korley, L. T. J. Confinement of Elastomeric Block Copolymers via Forced Assembly Co-extrusion. *ACS Appl. Mater. Interfaces* **2011**, *3* (12), 4804−4811.
(5) Burt, T. M.; Jordan, A. M.; Korley, L. T. J. Towards Anisotropic Materials via Forced Assembly Co-extrusion. *ACS Appl. Mater. Interfaces* **2012**, *4* (10), 5155−5161.
(6) Burt, T. M.; Jordan, A. M.; Korley, L. T. J. Investigating Interfacial Contributions on the Layer-thickness Dependent Mechanical Response of Confined Self-assembly via Forced Assembly. *Macromol. Chem. Phys.* **2013**, *214* (8), 873−881.
(7) Mackey, M.; Hiltner, A.; Baer, E.; Flandin, L.; Wolak, M. A.; Shirk, J. S. J. Enhanced breakdown strength of multilayered films fabricated by forced assembly microlayer coextrusion. *J. Phys. D: Appl. Phys.* **2009**, *42* (17), 175304 1−17530412.
(8) Kang, S. J.; Bae, I.; Park, Y. J.; Park, T. H.; Sung, J.; Yoon, S. C.; Kim, K. H.; Choi, D. H.; Park, C. Non-volatile Ferroelectric Poly(vinylidene fluoride-*co*-trifluoroethylene) Memory Based on a Single-Crystalline Tri-isopropylsilylethynyl Pentacene Field-Effect Transistor. *Adv. Funct. Mater.* **2009**, *19* (10), 1609−1616.
(9) Nalwa, H. S. *Ferroelectric Polymers: Chemistry: Physics, and Applications*; CRC Press: New York, 1995; Vol. *XII*, p 895.
(10) Lai, C. Y.; Hiltner, A.; Baer, E.; Korley, L. T. J. The Deformation of Confined Poly(ethylene oxide) in Multilayer Films. *ACS Appl. Mater. Interfaces* **2012**, *4* (4), 2218−2227.
(11) Lai, C. Y.; Ayyer, R.; Hiltner, A.; Baer, E. Effect of confinement on the relaxation behavior of poly(ethylene oxide). *Polymer* **2010**, *51* (8), 1820−1829.
(12) Koo, C. M.; Wu, L.; Lim, L. S.; Mahanthappa, M. K.; Hillmyer, M. A.; Bates, F. S. Microstructure and Mechanical Properties of Semicrystalline−Rubbery−Semicrystalline Triblock Copolymers. *Macromolecules* **2005**, *38* (14), 6090−6098.
(13) Martin, C. R. Nanomaterials: A Membrane-Based Synthetic Approach. *Science* **1994**, *266* (5193), 1961−1966.
(14) Steinhart, M.; Wehrspohn, R. B.; Gösele, U.; Wendorff, J. H. Nanotubes by Template Wetting: A Modular Assembly System. *Angew. Chem., Int. Ed.* **2004**, *43* (11), 1334−1344.
(15) Kamperman, M.; Korley, L. T. J.; Yau, B.; Johansen, K. M.; Joo, Y. L.; Wiesner, U. Nanomanufacturing of continuous composite nanofibers with confinement-induced morphologies. *Polym. Chem.* **2010**, *7* (1), 1001−1004.
(16) Kalra, V.; Mendez, S.; Lee, J. H.; Nguyen, H.; Marquez, M.; Joo, Y. L. Confined Assembly in Coaxially Electrospun Block Copolymer Fibers. *Adv. Mater.* **2006**, *18* (24), 3299−3303.
(17) Huang, P.; Zhu, L.; Guo, Y.; Ge, Q.; Jing, A. J.; Chen, W. Y.; Quirk, R. P.; Cheng, S. Z. D.; Thomas, E. L.; Lotz, B.; Hsiao, B. S.; Avila-Orta, C. A.; Sics, I. Confinement size effect on orientation changes of poly(ethylene oxide) crystals in poly(ethylene oxide)-*block*-polystyrene diblock copolymers. *Macromolecules* **2004**, *37* (10), 3689−3698.
(18) Liu, R. Y. F.; Jin, Y.; Hiltner, A.; Baer, E. Probing Nanoscale Polymer Interactions by Forced-Assembly. *Macromol. Rapid Commun.* **2004**, *24* (16), 943−948.
(19) Liu, R. Y. F.; Bernal-Lara, T. E.; Hiltner, A.; Baer, E. Polymer Interphase Materials by Forced Assembly. *Macromolecules* **2005**, *38* (11), 4819−4827.
(20) Toki, S.; Sics, I.; Ran, S.; Liu, L.; Murakami, S.; Senoo, K.; Kohijiya, S.; Hsiao, B. S. New Insights into Structural Development in Natural Rubber during Uniaxial Deformation by In Situ Synchrotron X-ray Diffraction. *Macromolecules* **2002**, *35* (17), 6578−6584.
(21) Blundell, D. J.; MacKerron, D. H.; Fuller, W.; Mahendrasignam, A.; Martin, C.; Oldman, R. J.; Rule, R. J.; Riekel, C. Characterization of strain-induced crystallization of poly(ethylene terephthalate) at fast draw rates using synchrotron radiation. *Polymer* **1996**, *37* (15), 3303−3311.
(22) Gorlier, E.; Haudin, J. M.; Billon, N. Strain-induced crystallisation in bulk amorphous PET under uni-axial loading. *Polymer* **2001**, *42* (23), 9541−9549.
(23) Todorov, L. V.; Viana, J. C. Structure evolution of PET under step-wise and continuous deformation modes: The effect of stress relaxation on the strain-induced morphology. *Int. J. Mater. Form.* **2008**, *1* (Suppl. 1), 661−665.
(24) Garcia-Gutierrez, M. C.; Linares, A.; Hernandez, J. J.; Rueda, D. R.; Ezquerra, T. A.; Poza, P.; Davies, R. J. Confinement-Induced One-Dimensional Ferroelectric Polymer Arrays. *Nano Lett.* **2010**, *10* (4), 1472−1476.
(25) Hiltner, A.; Baer, E.; Yijian, L.; Carr, J. M. Axially oriented confined crystallization multilayer films. U.S. Patent US20110241245 A1, Oct 06, 2011.
(26) Carr, J. M.; Mackey, M.; Flandin, L.; Hiltner, A.; Baer, E. Structure and transport properties of polyethylene terephthalate and poly(vinylidene fluoride-*co*-tetrafluoroethylene) multilayer films. *Polymer* **2013**, *54* (6), 1679−1690.
(27) Wang, H.; Keum, J. K.; Hiltner, A.; Baer, E.; Freeman, B.; Rozanski, A.; Galeski, A. Confined Crystallization of Polyethylene Oxide in Nanolayer Assemblies. *Science* **2009**, *323* (5915), 757−760.
(28) Carr, J. M.; Mackey, M.; Flandin, L.; Schuele, E.; Zhu, L.; Baer, E. Effect of biaxial orientation on dielectric and breakdown properties of poly(ethylene terephthalate)/poly(vinylidene fluoride-*co*-tetrafluoroethylene) multilayer films. *J. Polym. Sci., Part B: Polym. Phys.* **2013**, *51* (11), 882−896.
(29) Ponting, M.; Hiltner, A.; Baer, E. Polymer Nanostructures by Forced Assembly: Process, Structure, and Properties. *Macromol. Symp.* **2010**, *294* (1), 19−32.
(30) ASTM International. *Standard Test Method for Tensile Properties of Plastics; ASTM D638*; ASTM International: West Conshohocken, PA, 2010.
(31) Liu, R. Y. F.; Schiraldi, D. A.; Hiltner, A.; Baer, E. Oxygen-barrier properties of cold-drawn polyesters. *J. Polym. Sci., Part B: Polym. Phys.* **2002**, *40* (9), 862−877.
(32) Branciforti, M. C.; Sencadas, V.; Lanceros-Mendez, S.; Gregorio, R., Jr. New technique of processing highly oriented poly(vinylidene fluoride) films exclusively in the β phase. *J. Polym. Sci., Part B: Polym. Phys.* **2007**, *45* (19), 2793−2801.
(33) Kolbuck, D.; Sajkiewicz, P.; Maniura-Weber, K.; Fortunato, G. Structure and morphology of electrospun polycaprolactone/gelatine nanofibres. *Eur. Polym. J.* **2013**, *49* (8), 2052−2061.
(34) Tobolsky, A. V. Physics of Semicrystalline Polymers. *J. Chem. Phys.* **1962**, *37* (5), 1139−1145.
(35) Nielsen, L. E.; Stockton, F. D. Theory of the modulus of crystalline polymers. *J. Polym. Sci., Part A: Gen. Pap.* **1963**, *1* (6), 1995−2002.